

Impact of Many-Body Effects on Landau Levels in Graphene

J. Sonntag,^{1,2} S. Reichardt,^{1,3} L. Wirtz,³ B. Beschoten,¹ M. I. Katsnelson,⁴ F. Libisch,⁵ and C. Stampfer^{1,2}

¹*JARA-FIT and 2nd Institute of Physics, RWTH Aachen University, 52074 Aachen, Germany*

²*Peter Grünberg Institute (PGI-9), Forschungszentrum Jülich, 52425 Jülich, Germany*

³*Physics and Materials Science Research Unit, University of Luxembourg, L-1511 Luxembourg, Luxembourg*

⁴*Radboud University, Institute for Molecules and Materials, 6525AJ Nijmegen, Netherlands*

⁵*Institute for Theoretical Physics, Vienna University of Technology, 1040 Vienna, Austria*

(Dated: February 22, 2018)

We present magneto-Raman spectroscopy measurements on suspended graphene to investigate the charge carrier density-dependent electron-electron interaction in the presence of Landau levels. Utilizing gate-tunable magneto-phonon resonances, we extract the charge carrier density dependence of the Landau level transition energies and the associated effective Fermi velocity v_F . In contrast to the logarithmic divergence of v_F at zero magnetic field, we find a piecewise linear scaling of v_F as a function of charge carrier density, due to a magnetic field-induced suppression of the long-range Coulomb interaction. We quantitatively confirm our experimental findings by performing tight-binding calculations on the level of the Hartree-Fock approximation, which also allow us to estimate an excitonic binding energy of ≈ 6 meV contained in the experimentally extracted Landau level transition energies.

Many-body interactions crucially influence the electronic properties of graphene [1]. They are essential to the understanding of such effects as unconventional quantum Hall states [2, 3], graphene plasmonics [4–6] or the formation of a viscous Dirac fermion liquid [7, 8]. In particular, the long-range electron-electron interaction is predicted to heavily modify the single-particle band structure close to the charge neutrality point (CNP), which is described by a logarithmically divergent effective Fermi velocity v_F [9–12]. This charge carrier density (n_{el})-dependent band structure renormalization at low or vanishing magnetic fields was experimentally confirmed with various different experimental techniques such as, transport measurements [13], quantum capacitance measurements [14], angle-resolved photoemission spectroscopy (ARPES) [15, 16], and scanning tunneling spectroscopy [17, 18]. Still, very little is known about the effects of electron-electron interaction on the band structure of graphene in the presence of quantizing magnetic fields, i.e., Landau levels (LLs). The only experimental [19] and theoretical [20] studies so far focused on the scaling of the effective Fermi velocity with magnetic field at fixed charge carrier density close to the CNP. Interestingly, the extracted v_F is not in agreement with earlier experiments at low magnetic fields [13, 14] and hint toward a non-divergent behavior at the CNP. This raises the question whether the n_{el} -dependent renormalization of v_F and thus the many-body effects are fundamentally different in the presence of LLs.

In this Letter, we report on extracting the renormalized LL energies and the corresponding v_F as a function of charge carrier density n_{el} by optically probing gate-tunable magneto-phonon resonances in suspended graphene. Magneto-Raman spectroscopy has successfully been used to probe inter-LL excitations in graphene [19, 21–31] and allow the study of the electron-phonon

coupling and excitation lifetimes. Most importantly, this technique offers a suitable energy scale for measuring the B -field-tunable LL transition energies in the form of the Raman G mode phonon energy (≈ 196 meV). Typically, such energy scales characteristic for LLs are difficult to reach by thermally activated transport, which is the method of choice for extracting the energy-band or v_F renormalization at negligible B -field [13].

To compare the renormalization effects at low and high B -fields respectively, it is convenient to introduce an effective Fermi velocity v_F for high magnetic fields, which captures the complete renormalization of the LL energies due to many body-effects [32]. Thus, the unique square root dependence of the LL spectrum of massless Dirac fermions has to be modified with a renormalized effective Fermi velocity v_F , which now depends on B , n_{el} , and the LL index $\pm n$. The LL spectrum including many-body interactions thus reads: $\varepsilon_{\pm n} = \pm v_{F,n}(B, n_{\text{el}}) \sqrt{2\hbar B n}$. Most interestingly, our study of magneto-phonon resonances (MPRs) as a function of n_{el} reveals that the effective Fermi velocity does not scale logarithmically with n_{el} , as it is the case for $B \approx 0$ T, but rather shows a linear and thus finite dependence. We attribute this change in behavior to the suppression of the long-range Coulomb interaction for distances much larger than the magnetic length $l_B = \sqrt{\hbar/(eB)}$. Moreover, we present a quantitative description of the evolution of v_F in the presence of LLs within a tight-binding model [33] on the level of the Hartree-Fock approximation, finding a near-perfect agreement with our measurements.

For our experimental study, we use a current-annealed suspended graphene device offering high carrier mobility, low intrinsic strain, low charge carrier density inhomogeneity, and electron-electron interactions that are not screened by the environment. The device consists of a graphene flake on a Si/SiO₂ substrate which was exfoli-

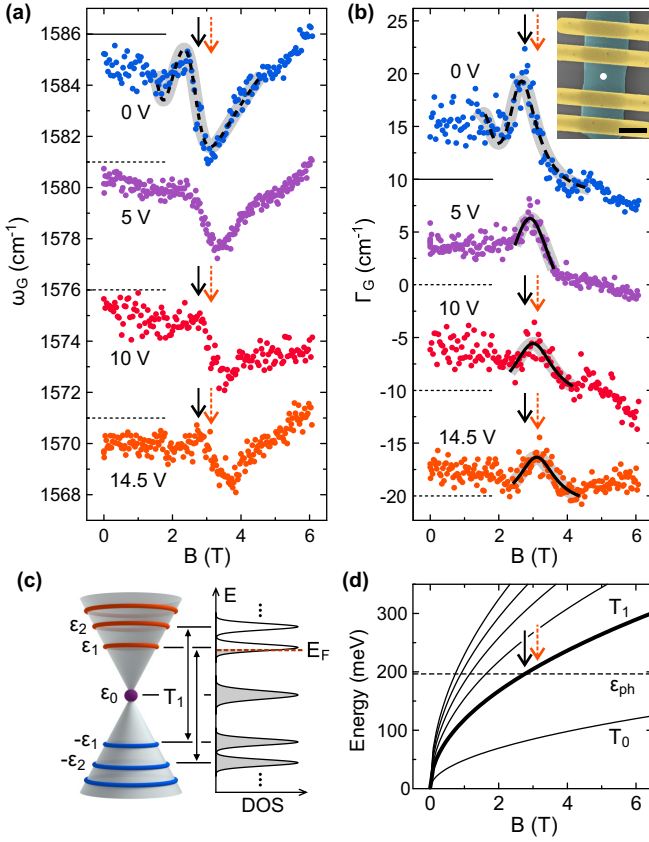


FIG. 1. The position (a) and width (b) of the Raman G peak as a function of the magnetic field for different gate voltages. For clarity the graphs are each offset by 5 cm^{-1} and 10 cm^{-1} , respectively (horizontal dashed lines). The solid, black and dashed, orange arrows illustrate the shift of the T_1 -MPR position from $V_g = 0 \text{ V}$ to $V_g = 14.5 \text{ V}$, corresponding to $n_{\text{el}} \approx 0 \text{ cm}^{-2}$ and $n_{\text{el}} \approx 0.5 \times 10^{12} \text{ cm}^{-2}$, respectively. The dashed curves in the upper-most trace represent the theoretical model of MPRs presented in the Supplemental Material [34]. The solid curves depict Lorentzian fits to Γ_G close to the resonance. The inset depicts a false-color scanning electron micrograph of the measured device. The white circle portrays our laser spot and the scale bar represents $2 \mu\text{m}$. (c) Schematic illustration of the density of states, the Fermi energy E_F , and the relevant interband LL transition T_1 . (d) Interband LL transition energies T_n , assuming an effective $v_F = 1.35 \times 10^6 \text{ m/s}$. The dashed line indicates the energy of the G mode phonon at $B = 0 \text{ T}$.

ated, contacted with Cr/Au contacts, and suspended by etching away $\approx 160 \text{ nm}$ of SiO_2 . A subsequent current annealing step effectively cleans the graphene [35], giving rise to a carrier mobility exceeding $400\,000 \text{ cm}^2/(\text{Vs})$ and a charge inhomogeneity of less than $n^* \approx 10^9 \text{ cm}^{-2}$ (see Supplemental Material [34]), which allow the observation of magneto-phonon resonances below 4 T [22–30]. The Si back gate moreover permits the controlled tuning of the charge carrier density, as well as electrical feedthroughs. This permits combined optical and transport experiments. We use linearly polarized laser light

with an excitation wavelength of 532 nm , a laser power of 0.5 mW , and a spot size of $\approx 500 \text{ nm}$. For the detection of the scattered light, we employ a CCD spectrometer with a grating of 1200 lines/mm . All measurements were performed at a temperature of 4.2 K .

To study magneto-phonon resonances as a function of charge carrier density, we vary $n_{\text{el}} = \alpha \cdot (V_g - V_0)$ by tuning the applied gate voltage V_g , where $V_0 = -0.2 \text{ V}$ accounts for the residual doping. We extract the lever-arm $\alpha = 3.15 \times 10^{10} \text{ cm}^{-2} \text{ V}^{-1}$ from a Landau fan measurement (see Supplemental Material [34]). For each specific V_g , we sweep the magnetic field from 0 T to 6 T , while recording the Raman spectrum. To study the coupling of the electronic system to the Raman-active E_{2g} mode, we extract the position ω_G and width Γ_G of the Raman G peak by fitting a single Lorentzian. Their evolution as a function of B -field for different values of V_g is shown in Fig. 1a and b, respectively. We observe the resonant coupling of the Raman G mode phonon [22–28] to electronic transitions when its bare energy $\epsilon_{\text{ph}} = \hbar\omega_G(B = 0 \text{ T}, n_{\text{el}} = 0 \text{ cm}^{-2}) \equiv \hbar\omega_0$ matches the energy of a transition between the discrete LLs. Most prominently, this coupling results in a decrease of the phonon lifetime due to the excitation of electron-hole pairs, which results in an increased width Γ_G of the Raman G peak at resonance. To first order in perturbation theory, the E_{2g} -phonon only couples to LL excitations with $\Delta n = \pm 1$ [29, 30]. We thus focus on the coupling to LL transitions whose energies are given by $T_n = \epsilon_{n+1} - \epsilon_{-n}$ (see Fig. 1c and d). Note that the influence of excitonic effects on T_n is neglected here and will be discussed later in this Letter. The resonance condition $\epsilon_{\text{ph}} = T_n$ can be expressed as:

$$\hbar\omega_0 = v_{F,T_n}(B_{T_n}, n_{\text{el}}) \sqrt{2e\hbar B_{T_n}} (\sqrt{n+1} + \sqrt{n}), \quad (1)$$

where we defined an effective Fermi velocity v_{F,T_n} of the transition T_n via $v_{F,T_n} \equiv T_n / (\sqrt{2e\hbar B} (\sqrt{n+1} + \sqrt{n}))$ [36]. By measuring ω_0 and the value of the B -field at which the resonance occurs, B_{T_n} , one can thus extract the effective Fermi velocity $v_{F,T_n}(B = B_{T_n}, n_{\text{el}})$. The experimentally determined v_{F,T_n} evidently contains all corrections from electron-electron interactions. Hence the position of the magneto-phonon resonance provides a direct probe of the renormalized transition energy, parametrized by an effective Fermi velocity. In particular, we are able to probe the charge carrier density dependence of v_{F,T_n} by varying V_g .

In the following, we focus on the charge carrier density dependence of the T_1 transition [28–30], which gives rise to a resonance at $B_{T_1} \approx 3 \text{ T}$ (Fig. 1a and b). Increasing the charge carrier density leads both to an increase of B_{T_1} (compare black and red arrows in Fig. 1a and b) and to a decrease of the strength of the T_1 -MPR, which we define as the maximum value of Γ_G at the resonance B_{T_1} , $\Gamma_{G,T_1}^{\text{max}}$. For a more quantitative analysis, we fit single Lorentzians

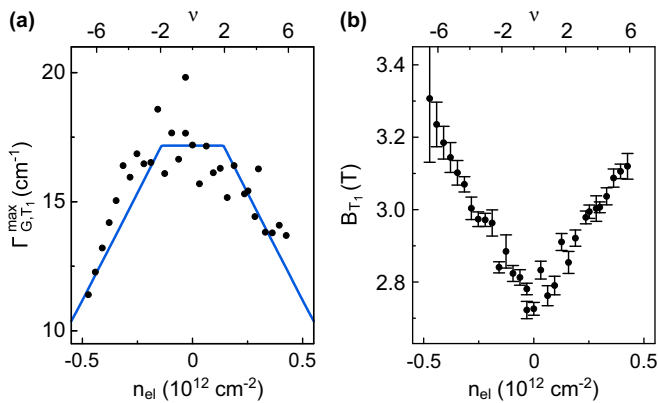


FIG. 2. (a) Peak width of the G mode at the T_1 -resonance as a function of charge carrier density. The blue line represents the theoretical prediction obtained with the average parameters of all measurements. (b) Charge carrier density-dependent position B_{T_1} of the T_1 -resonance. The change in B_{T_1} indicates a change in v_{F,T_1} . The upper axis shows the filling factor ν at $B = 3$ T.

to Γ_G (Fig. 1b) as a function of B around the T_1 -MPR to obtain Γ_{G,T_1}^{\max} and B_{T_1} (see Fig. 2a and b). The observed behavior of Γ_{G,T_1}^{\max} with n_{el} can be understood in terms of the increasing filling of different LLs and the resulting Pauli blocking. For small $|n_{el}|$, the Fermi energy stays within the zeroth LL and hence Γ_{G,T_1}^{\max} remains almost constant, as the T_1 transition involves only the transitions $-1 \rightarrow +2$ and $-2 \rightarrow +1$. For higher values of $|n_{el}|$, the states belonging to the first LL are increasingly filled up and more and more of the degenerate LL-transitions become blocked. The decrease of Γ_{G,T_1}^{\max} with $|n_{el}|$ is in good agreement with the theoretical prediction (blue line in Fig. 2a, also see Supplementary Material [34]), while the linear scaling can be understood from the linear scaling of the filling factor ν with n_{el} (see below).

Next, we analyze the charge carrier density dependence of the position B_{T_1} of the T_1 -MPR (see Fig. 2b). According to Eq. 1, B_{T_1} only depends on the value of the phonon frequency ω_0 and on v_{F,T_1} . We rule out changes of ω_0 due to tensile strain from electrostatically pulling the graphene flake as the origin of the observed shift in B_{T_1} , since the observed variation of ω_0 is negligible (less than 2 cm^{-1} , also see Supplementary Material [34]). Furthermore, tensile strain would *soften* ω_0 , i.e., it would lead to a *decrease* of B_{T_1} with increasing n_{el} . Thus, the shift of B_{T_1} can only be caused by a change of the LL excitation energies, as described by an n_{el} -dependent effective Fermi velocity v_{F,T_1} . For a quantitative analysis of $v_{F,T_1}(n_{el})$, we employ Eq. 1 and the extracted B_{T_1} to directly calculate v_F as a function of n_{el} (see Fig. 3). We obtain an effective Fermi velocity ranging from $v_{F,T_1} \approx 1.36 \times 10^6 \text{ m/s}$ close to the charge neutrality point to $v_{F,T_1} \approx 1.24 \times 10^6 \text{ m/s}$ at a charge carrier density of $|n_{el}| = 0.4 \times 10^{12} \text{ cm}^{-2}$. Most interestingly, we

do not observe a logarithmically divergent behavior close to the CNP, as it is the case in the low B -field regime (see inset in Fig. 3) [13, 14]. Instead, we find a finite, linear decrease of v_{F,T_1} as a function of $|n_{el}|$. We attribute this linear behavior to the degeneracy of the states within one LL. Due to the degeneracy, the contribution of a certain LL to the renormalization of v_{F,T_1} effectively equals the sum of the contributions of all its states weighted by the filling of the LL. Since the partial filling factor scales linearly with n_{el} , so does the renormalization of v_{F,T_1} , as long as n_{el} is varied in a range for which the Fermi level E_F stays within a single LL. When E_F enters a different LL, the slope of v_{F,T_1} changes as a different LL is now filled up and its contribution is added.

We confirm this qualitative argument and the experimental observation by quantitative calculations on the level of the Hartree-Fock approximation (HFA) within a tight-binding model [33] (see Supplementary Material [34]). In the HFA, the single-particle LL energies are renormalized by contributions from all occupied states via the direct Coulomb (Hartree term) and exchange interactions (Fock term): $\varepsilon_n(B, n_{el}) = \varepsilon_n^0(B) + \Sigma_n^{\text{HF}}(B, n_{el})$, where ε_n^0 denotes the bare value of the LL energies and

$$\begin{aligned} \Sigma_n^{\text{HF}}(B, n_{el}) &= \frac{1}{N_m} \sum_m \Sigma_{n,m}^{\text{HF}}(B, n_{el}) \\ &= \frac{1}{N_m} \sum_m \sum_{n',m'} \bar{v}_{n'}(B, n_{el}) \begin{pmatrix} 2v_{(n,m),(n',m')}^{\text{Hart.}}(B) & v_{(n,m),(n',m')}^{\text{Fock}}(B) \end{pmatrix} \end{aligned} \quad (2)$$

is the self-energy of LL n in the HFA, averaged over all N_m degenerate states, labeled by the quantum number m [37], and $v_{(n,m),(n',m')}^{\text{Hart.},\text{Fock}}(B)$ represent the direct Coulomb and exchange matrix elements, respectively, between the LL states $|n, m\rangle$ and $|n', m'\rangle$. Finally, $\bar{v}_n(B, n_{el}) = n_{el}h/(4eB) - n + 1/2$ denotes the partial filling factor of LL n , which is set to 0 (1) for $\bar{v}_n < 0$ (> 1) and equals the occupancy of LL n . Including the Hartree-Fock correction, the energy of the T_n -transition reads

$$T_n(B, n_{el}) = \varepsilon_{n+1}^0 - \varepsilon_{-n}^0 + \Sigma_{n+1}^{\text{HF}} - \Sigma_{-n}^{\text{HF}}. \quad (3)$$

To account for the intrinsic screening of the graphene sheet, we use an effective dielectric constant of $\epsilon = 3.1$ to screen all Coulomb matrix elements by an additional factor of $1/\epsilon$, in agreement with earlier work [13]. Expressing $T_n(B, n_{el})$ in terms of the effective Fermi velocity v_{F,T_n} (compare Eq. 1), Eq. 3 implies

$$v_{F,T_n}(n_{el}) = v_{F,T_n}(n_{el}^0) + \frac{\Delta \Sigma_{n+1}^{\text{HF}}(n_{el}) - \Delta \Sigma_{-n}^{\text{HF}}(n_{el})}{\sqrt{2e\hbar B T_n}(\sqrt{n+1} + \sqrt{n})}, \quad (4)$$

where $\Delta \Sigma_n^{\text{HF}}(n_{el}) = \Sigma_n^{\text{HF}}(n_{el}) - \Sigma_n^{\text{HF}}(n_{el}^0)$ denotes the difference in self-energies and $n_{el}^0 = 0 \text{ cm}^{-2}$. Note that in this difference, all contributions from states outside the

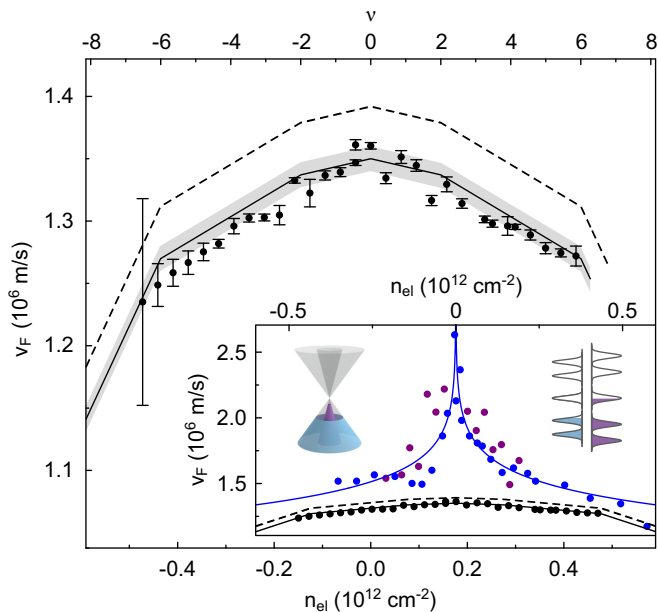


FIG. 3. The effective Fermi velocity as extracted from the T_1 -resonance as a function of charge carrier density. The upper axis shows the filling factor ν at $B = 3$ T. The solid black (dashed) line shows the calculated renormalization of v_{F,T_1} without (with) considering the excitonic binding energy. The grey-shaded area illustrates the uncertainty due to the B -field-dependent renormalization of v_F [21, 38]. The inset shows a comparison between v_F in the presence of Landau levels (black dots from MPRs, black lines calculated) and at low magnetic field (blue and purple dots). The blue data points are taken from Elias *et al.* [13], while the purple dots represent v_F as extracted from temperature-dependent SdHO measurements on the graphene device presented in this study. The blue line shows the expected logarithmic renormalization at low magnetic fields. The two sketches illustrate the n_{el} -induced renormalization of the energy spectrum for low (left) and high (right) magnetic fields.

energy window defined by n_{el}^0 and n_{el} drop out for constant magnetic field, as their occupancies do not change. This applies in particular to contributions from states beyond the UV cutoff in renormalization group approaches [9, 10, 13], which correspond to contributions from states deep inside the valence band. These states only influence the overall scale of v_F , which is set by the value of $v_{F,T_1}(n_{el}^0)$. For our calculation, we use the experimentally extracted value of $v_{F,T_1}(n_{el}^0) = 1.35 \times 10^6$ m/s as input. As seen in Fig. 3, our calculation predicts a piecewise-linear $v_F(n_{el})$, which is in excellent agreement with our experimental results [38] and very recent theoretical work [39].

In order to compare v_{F,T_1} with measurements of the effective Fermi velocity at low magnetic fields extracted by transport experiments [13, 14], it is important to discuss the so far neglected excitonic effects in our MPR analysis. As we probe electron-hole pair excitations, the experimentally extracted LL transition energies $T_n = \varepsilon_{n+1} -$

$\varepsilon_{-n} + \varepsilon_{n+1,-n}^{\text{bind.}}$ include a (negative) binding energy of the electron-hole pair $\varepsilon_{n+1,-n}^{\text{bind.}}$. Consequently, our experimentally extracted $v_{F,T_1}(n_{el}^0)$ already contains an excitonic component of $\delta v_{F,T_1}^{\text{bind.}} = \varepsilon_{2,-1}^{\text{bind.}} / (\sqrt{2}e\hbar B(\sqrt{2} + 1))$ (compare Eq. 1). To correct for the excitonic effects and thus permit a sensible comparison to the v_F extracted from transport measurements, we estimate $\varepsilon_{n+1,-n}^{\text{bind.}}$ by approximating it within our HFA tight-binding model as the difference of the direct and exchange Coulomb matrix elements, averaged over all possible pairs of degenerate LL states:

$$\varepsilon_{n+1,-n}^{\text{bind.}} = 1/N_m^2 \sum_{m,m'} \begin{pmatrix} v_{(n+1,m)}^{\text{Hart.}} & -v_{(n+1,m)}^{\text{Fock}} \\ \varepsilon_{(-n,m')} & \varepsilon_{(-n,m')} \end{pmatrix}. \quad (5)$$

The numerical evaluation of this expression yields an n_{el} -independent estimate of $\varepsilon_{2,-1}^{\text{bind.}} \approx -6$ meV, when including the screening factor of $1/\varepsilon$. When correcting v_{F,T_1} for $\delta v_{F,T_1}^{\text{bind.}}$, we obtain values for the effective Fermi velocity without any excitonic effects, as shown as the black dotted line in Fig. 3.

The inset in Fig. 3 shows a comparison of v_F at low magnetic fields (< 0.5 T) and in the presence of LLs (≈ 3 T). The purple dots represent $v_F(n_{el})$ at low magnetic fields, extracted from temperature-dependent Shubnikov-de Haas oscillation (SdHO) measurements (see Supplemental Material [34]) taken on the very same device used for our MPR study. They are in good agreement with the previously reported v_F by Elias *et al.* [13] (blue dots) and the expected logarithmic behavior at low magnetic fields (blue line). Most interestingly, there is a striking difference in the n_{el} -dependence between v_F extracted at low magnetic fields from transport experiments and v_{F,T_1} determined at high magnetic fields from our optical measurements. Note that the magneto-Raman measurements always probe v_F away from the Dirac point at approximately half the phonon energy (≈ 100 meV), while transport experiments extract the band slope at the Fermi surface. However, previous ARPES [16] and scanning tunneling spectroscopy [17] studies established that the renormalized bands remain linear within an energy window around the CNP of at least 200 meV (see left schematic in inset Fig. 3). As we both probe v_F and tune the Fermi energy within this energy window, the exact energy at which v_F is probed is irrelevant. Consequently, it is justified to compare our results to the ones from transport measurements at low B -fields. Since the excitonic correction cannot account for the change in effective Fermi velocities between the two techniques, we conclude that the difference in v_F is *not* due to the way in which v_F is determined, but rather due to the difference in electron-electron interaction at low B -fields and in the presence of LLs. At low magnetic fields, the self-energy correction to v_F diverges due to the long-range behavior of the Coulomb interaction and the delocalized nature of the Dirac electrons at the K point. By contrast, high

magnetic fields exponentially localize the electronic wave functions once LLs are present, with a decay constant on the order of the magnetic length l_B (see Supplementary Material [34]). As a result, the long-range divergence is eliminated.

In conclusion, we extracted the charge carrier density dependence of the effective Fermi velocity close to the charge neutrality point in the presence of LLs by studying magneto-phonon resonances. In contrast to the logarithmic renormalization of v_F found at low magnetic fields, we find that in the LL regime v_F stays finite and scales piecewise linearly with n_{el} . The linear scaling of v_F with n_{el} originates from the degeneracy of the LLs. By contrast, the suppression of the divergence at the charge neutrality point can be traced back to the spatial confinement of the electron wave functions by the magnetic field, which cuts off the divergent long-range Fock contribution. Tight-binding calculations based on the Hartree-Fock approximation quantitatively verify our experimental findings and confirm that electron-electron interactions in graphene are indeed very sensitive to the applied magnetic field and that they can change dramatically for different magnetic field regimes. The general nature of the gained insight into many-body effects on the electronic excitation energies in strong magnetic fields make them applicable to the study of other low-dimensional materials as well and can be of great value for the effective tuning of material properties.

We thank C. Neumann, E. Andrei, and F. Guinea for helpful discussions and M. Goldsche for help with sample fabrication. Support by the ERC (GA-Nr. 280140), the Helmholtz Nano Facility [40], the DFG, and the European Unions Horizon 2020 programme under grant agreement No 696656 (Graphene Flagship) are gratefully acknowledged. S.R. and L.W. acknowledge financial support by the National Research Fund (FNR) Luxembourg (projects RAMGRASEA and TMD-nano: INTER/ANR/13/20/NANOTMD). F.L. acknowledges financial support by the FWF (SFB-F41 ViCoM) and numerical support by the Vienna Scientific Cluster (VSC).

[1] V. N. Kotov, B. Uchoa, V. M. Pereira, F. Guinea, and A. H. Castro Neto, *Rev. Mod. Phys.* **84**, 1067 (2012).
 [2] C. Dean, A. Young, P. Cadden-zimansky, L. Wang, H. Ren, K. Watanabe, T. Taniguchi, P. Kim, J. Hone, and K. Shepard, *Nat. Phys.* **7**, 693 (2011).
 [3] A. Young, C. Dean, L. Wang, H. Ren, P. Cadden-Zimansky, K. Watanabe, T. Taniguchi, J. Hone, K. Shepard, and P. Kim, *Nat. Phys.* **8**, 550 (2012).
 [4] A. N. Grigorenko, M. Polini, and K. S. Novoselov, *Nat. Photonics* **6**, 749 (2012).
 [5] M. B. Lundberg, Y. Gao, R. Asgari, C. Tan, B. Van Duppen, M. Autore, P. Alonso-González, A. Woessner, K. Watanabe, T. Taniguchi, R. Hillenbrand, J. Hone, M. Polini, and F. H. L. Koppens, *Science*

357, 187 (2017).
 [6] D. N. Basov, M. M. Fogler, and F. J. García de Abajo, *Science* **354** (2016).
 [7] D. Bandurin, I. Torre, R. K. Kumar, M. B. Shalom, A. Tomadin, A. Principi, G. Auton, E. Khestanova, K. Novoselov, I. Grigorieva, L. Ponomarenko, A. Geim, and M. Polini, *Science* **351**, 1055 (2016).
 [8] J. Crossno, J. K. Shi, K. Wang, X. Liu, A. Harzheim, A. Lucas, S. Sachdev, P. Kim, T. Taniguchi, K. Watanabe, *et al.*, *Science* **351**, 1058 (2016).
 [9] J. González, F. Guinea, and M. Vozmediano, *Nucl. Phys. B* **424**, 595 (1994).
 [10] J. González, F. Guinea, and M. A. H. Vozmediano, *Phys. Rev. B* **59**, R2474 (1999).
 [11] T. Stauber, P. Parida, M. Trushin, M. V. Ulybyshev, D. L. Boyda, and J. Schliemann, *Phys. Rev. Lett.* **118**, 266801 (2017).
 [12] S. Das Sarma and E. H. Hwang, *Phys. Rev. B* **87**, 045425 (2013).
 [13] D. Elias, R. Gorbachev, A. Mayorov, S. Morozov, A. Zhukov, P. Blake, L. P. I. Grigorieva, K. Novoselov, F. Guinea, and A. Geim, *Nat. Phys.* **7**, 701 (2011).
 [14] G. Yu, R. Jalil, B. Belle, A. S. Mayorov, P. Blake, F. Schedin, S. V. Morozov, L. A. Ponomarenko, F. Chiappini, S. Wiedmann, U. Zeitler, M. Katsnelson, A. Geim, K. Novoselov, and D. Elias, *Proc. Natl. Acad. Sci. U.S.A.* **110**, 3282 (2013).
 [15] A. Bostwick, F. Speck, T. Seyller, K. Horn, M. Polini, R. Asgari, A. H. MacDonald, and E. Rotenberg, *Science* **328**, 999 (2010).
 [16] D. A. Siegel, C.-H. Park, C. Hwang, J. Deslippe, A. V. Fedorov, S. G. Louie, and A. Lanzara, *Proc. Natl. Acad. Sci. U.S.A.* **108**, 11365 (2011).
 [17] J. Chae, S. Jung, A. F. Young, C. R. Dean, L. Wang, Y. Gao, K. Watanabe, T. Taniguchi, J. Hone, K. L. Shepard, P. Kim, N. B. Zhitenev, and J. A. Stroscio, *Phys. Rev. Lett.* **109**, 116802 (2012).
 [18] A. Luican, G. Li, and E. Y. Andrei, *Phys. Rev. B* **83**, 041405 (2011).
 [19] C. Faugeras, S. Berciaud, P. Leszczynski, Y. Henni, K. Nogajewski, M. Orlita, T. Taniguchi, K. Watanabe, C. Forsythe, P. Kim, R. Jalil, A. Geim, D. Basko, and M. Potemski, *Phys. Rev. Lett.* **114**, 126804 (2015).
 [20] A. Sokolik, A. Zabolotskiy, and Y. E. Lozovik, *Phys. Rev. B* **95**, 125402 (2017).
 [21] C. Faugeras, P. Kossacki, A. Nicolet, M. Orlita, M. Potemski, A. Mahmood, and D. Basko, *New J. Phys.* **14**, 095007 (2012).
 [22] C. Neumann, D. Halpaap, S. Reichardt, L. Banszerus, M. Schmitz, K. Watanabe, T. Taniguchi, B. Beschoten, and C. Stampfer, *Appl. Phys. Lett.* **107**, 233105 (2015).
 [23] J. Yan, S. Goler, T. D. Rhone, M. Han, R. He, P. Kim, V. Pellegrini, and A. Pinczuk, *Phys. Rev. Lett.* **105**, 227401 (2010).
 [24] C. Faugeras, M. Amado, P. Kossacki, M. Orlita, M. Kühne, A. A. Nicolet, Y. I. Latyshev, and M. Potemski, *Phys. Rev. Lett.* **107**, 036807 (2011).
 [25] S. Goler, J. Yan, V. Pellegrini, and A. Pinczuk, *Solid State Commun.* **152**, 1289 (2012).
 [26] C. Faugeras, M. Amado, P. Kossacki, M. Orlita, M. Sprinkle, C. Berger, W. A. De Heer, and M. Potemski, *Phys. Rev. Lett.* **103**, 186803 (2009).
 [27] X. Shen, C. Qiu, B. Cao, C. Cong, W. Yang, H. Wang, and T. Yu, *Nano Research* **8**, 1139 (2015).

- [28] C. Neumann, S. Reichardt, M. Drögeler, B. Terrés, K. Watanabe, T. Taniguchi, B. Beschoten, S. V. Rotkin, and C. Stampfer, *Nano Lett.* **15**, 1547 (2015).
- [29] T. Ando, *J. Phys. Soc. Jpn.* **76**, 024712 (2007).
- [30] M. O. Goerbig, J.-N. Fuchs, K. Kechedzhi, and V. I. Fal'ko, *Phys. Rev. Lett.* **99**, 087402 (2007).
- [31] C. Faugeras, M. Orlita, and M. Potemski, *J. Raman Spectrosc.* (2017), 10.1002/jrs.5213.
- [32] Note that in this context the effective Fermi velocity $v_F = v_{F,n}(B, n_{el})$ is no longer linked to its definition as the slope of the energy bands, but rather directly describes the renormalization of the LL energies.
- [33] L. Chizhova, J. Burgdörfer, and F. Libisch, *Phys. Rev. B* **92**, 125411 (2015).
- [34] See Supplemental Material [URL will be inserted by publisher] for additional details on the tight-binding calculations, the model used to fit the MPRs and more detailed electrical characterisations.
- [35] K. I. Bolotin, K. Sikes, Z. Jiang, M. Klima, G. Fudenberg, J. Hone, P. Kim, and H. Stormer, *Solid State Commun.* **146**, 351 (2008).
- [36] In terms of the renormalized Fermi velocities $v_{F,n+1}$ and $v_{F,-n}$ of the respective Landau levels, the effective Fermi velocity of the T_n transition reads: $v_{F,T_n} = (v_{F,n+1}\sqrt{n+1} + v_{F,-n}\sqrt{n})/(\sqrt{n+1} + \sqrt{n})$.
- [37] The physical meaning of m depends on the choice of gauge for the vector potential. In Landau gauge, m represents the momentum in y -direction, while in symmetric gauge, m represents the z -component of the angular momentum.
- [38] Note that we experimentally extract v_{F,T_1} at slightly different B -fields for each value of n_{el} , due to the n_{el} -dependent renormalization of v_{F,T_1} . As shown previously [19], the effective Fermi velocity also exhibits a B -field-dependent renormalization proportional to $\log(B_2/B_1)$. However, the magnitude of this renormalization $\delta v_F \approx 0.02 \times 10^6$ m/s for the observed range of B_{T_1} -values (2.8 T to 3.2 T) is small compared to the n_{el} -induced corrections and hence we neglect it.
- [39] A. A. Sokolik and Y. E. Lozovik, *Phys. Rev. B* **97**, 075416 (2018).
- [40] W. Albrecht, J. Moers, and B. Hermanns, *Journal of large-scale research facilities* **3**, 112 (2017).
- [41] C. Lanczos, *An iteration method for the solution of the eigenvalue problem of linear differential and integral operators* (United States Governm. Press Office Los Angeles, CA, 1950).
- [42] S. Sharapov, V. Gusynin, and H. Beck, *Phys. Rev. B* **69**, 075104 (2004).
- [43] M. Katsnelson, *Graphene: Carbon in Two Dimensions* (Cambridge University Press, 2012).
- [44] N. Y. Astrakhantsev, V. V. Braguta, and M. I. Katsnelson, *Phys. Rev. B* **92**, 245105 (2015).
- [45] V. Gusynin, V. Miransky, and I. Shovkovy, *Physical Review D* **52**, 4718 (1995).

Supplemental Material: Impact of Many-Body Effects on Landau Levels in Graphene

THEORY OF MAGNETO-PHONON RESONANCES IN SINGLE-LAYER GRAPHENE

Following Ando [29], Goerbig *et al.* [30], and Neumann *et al.* [28], we calculate the Raman G mode phonon frequency ω_G and line width Γ_G as the real and doubled negative imaginary part, respectively, of the root of the following equation:

$$\omega^2 - (\omega_0 - i\gamma_0/2)^2 = 2(\omega_0 - i\gamma_0/2)\Pi(\omega), \quad (\text{S1})$$

where the phonon self-energy $\Pi(\omega)$ is given by

$$\Pi(\omega) = ev_F^2 B \lambda \sum_{n=0}^{\infty} \left[\frac{(\bar{\nu}_{-n} - \bar{\nu}_{n+1} - \bar{\nu}_n + \bar{\nu}_{-(n+1)}) (T_n - i\gamma_{el}/2)}{\omega^2 - (T_n - i\gamma_{el}/2)^2} + \frac{2}{T_n - i\gamma_{el}/2} \right]. \quad (\text{S2})$$

Here, $T_n = \frac{1}{\hbar} |\varepsilon_{n+1} + \varepsilon_n|$ are the frequencies associated with the inter-Landau level transitions, and $\varepsilon_{\pm n} = \pm v_{F,n} \sqrt{2e\hbar B n}$ is the energy of the $\pm n$ th Landau level as stated in the main text. $\bar{\nu}_n = (\nu - 4n + 2)/4$ denotes the partial filling factor, which depends on the filling factor $\nu = n_{el} h / (eB)$ and obeys $0 \leq \bar{\nu}_n \leq 1$. γ_{el} introduces a damping of the Landau level excitations to account for their finite lifetimes and γ_0 represents the damping of the phonon mode due to anharmonic effects. The dimensionless electron-phonon coupling constant is denoted by λ . By fitting the root of Eq. S1 to all our MPR measurements we get a set of average parameters leading to: $\omega_0 = 1584.8 \text{ cm}^{-1}$, $\gamma_0 = 7.6 \text{ cm}^{-1}$, $\gamma_{el} = 395 \text{ cm}^{-1}$, $\lambda = 4 \times 10^{-3}$ and $v_F = 1.33 \times 10^6 \text{ m/s}$, which we then use to calculate the maximum width Γ_{G,T_1}^{\max} at the resonance B_{T_1} as a function of charge carrier density, as represented by the blue line in Fig. 2a in the main text.

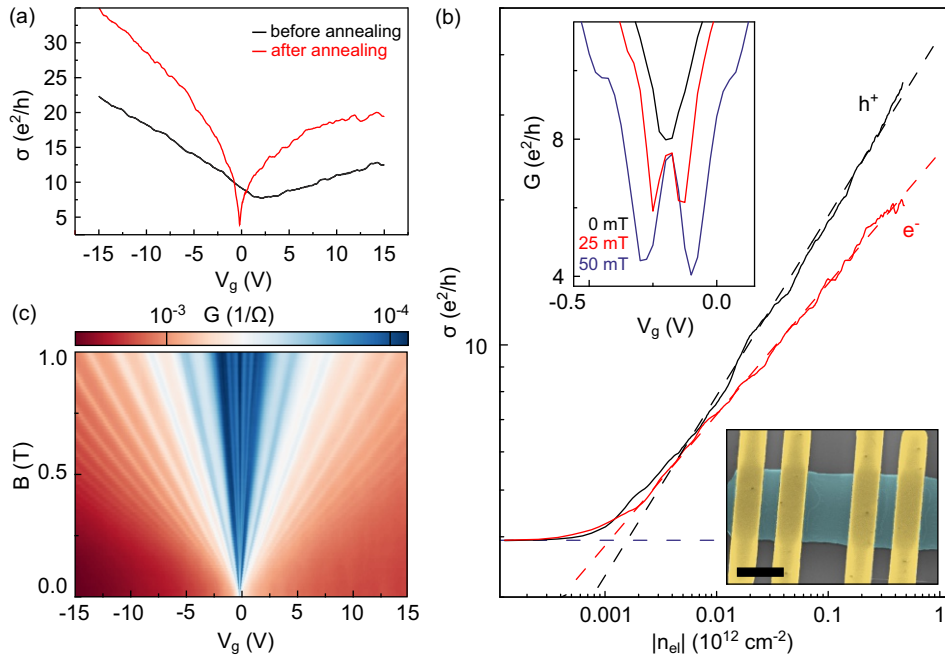


FIG. S1. (a) Electrical conductivity σ as a function of gate voltage V_g of the suspended graphene sample before and after current annealing. Measurements are taken at $T = 4.2 \text{ K}$. (b) Double logarithmic graph of the conductivity σ after current annealing as a function of charge carrier density for holes (black) and electrons (red). The red and black dashed lines are linear fits outside the regime of charge inhomogeneity. The purple, horizontal, dashed line indicates the minimum conductivity due to charge inhomogeneity. The crossing point of these lines defines n^* . The left inset shows the onset of SdHO at approx. 25 mT, indicating a mobility $\mu \approx 400\,000 \text{ cm}^2/(\text{Vs})$. The right inset depicts a false-color scanning electron micrograph of the measured device. The scale bar represents 2 μm . (c) Electrical conductivity as a function of magnetic field and gate voltage, used to determine back gate the lever-arm $\alpha = 3.15 \times 10^{10} \text{ cm}^{-2}\text{V}^{-1}$.

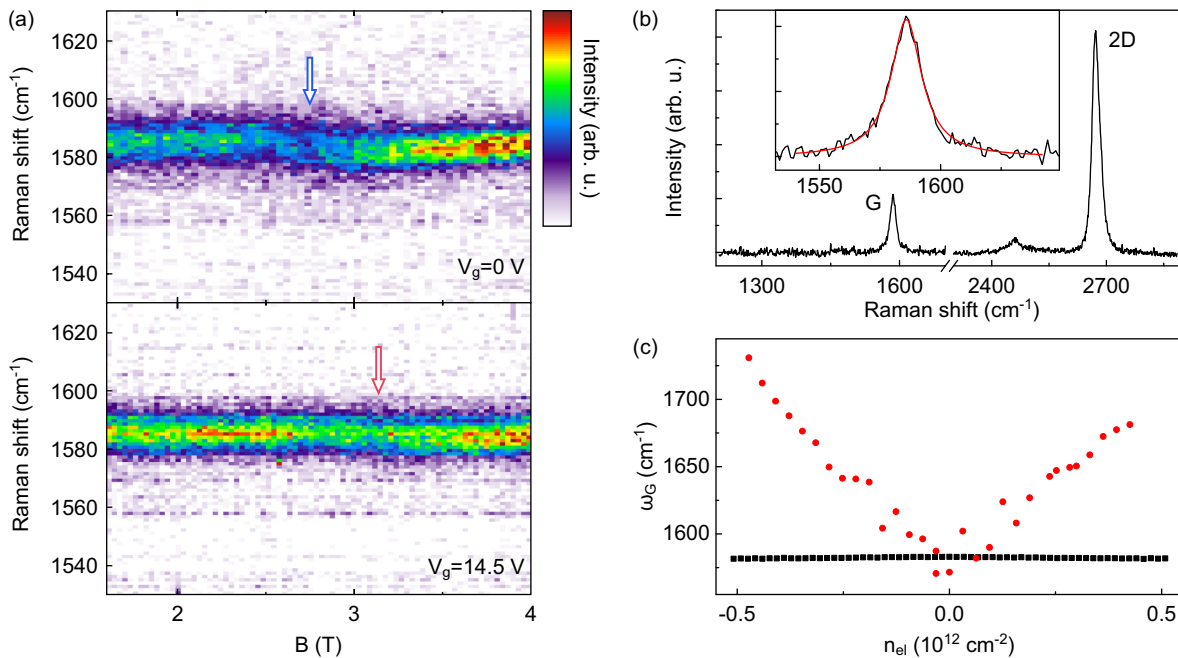


FIG. S2. (a) Raman intensity around the G peak plotted as a function of the magnetic field around the T_1 -MPR at $V_g = 0$ V and $V_g = 14.5$ V. The arrows indicate the positions of the T_1 -MPRs as extracted in the main text. (b) Raman spectrum taken at $V_g = 0$ V and $B = 0$ T. the inset depicts a Lorentzian fit of the G peak. (c) Illustration of the change in ω_G required to observe the shift in B_{T_1} as seen in Fig. 2 in the main text under the assumption of a constant $v_F = 1.06 \times 10^6$ m/s (red dots). Black squares represent the actually measured ω_G as a function of charge carrier density at zero magnetic field.

TIGHT-BINDING MODEL

We use a third-nearest neighbor tight-binding description of graphene [33] to evaluate the Coulomb and exchange contributions required for the self-energy correction $\Sigma_{\pm n}^{\text{HF}}$. We include the magnetic field via a Peierls phase factor and eliminate edge states by a finite mass boundary term at the zigzag edges [33]. We use an Arnoldy-Lanczos algorithm in conjunction with shift-invert [41] to calculate approximately 3000 eigenstates (in groups of 400 for efficiency) of a quadratic graphene flake of size 40×40 nm² at a magnetic field of 200 T. The Coulomb and exchange contributions are evaluated as

$$v_{i,j}^{\text{Hart.}} = e^2 \langle ij | \frac{1}{|\vec{r}_1 - \vec{r}_2|} |ij\rangle \quad (\text{S3})$$

and

$$v_{i,j}^{\text{Fock}} = e^2 \langle ji | \frac{1}{|\vec{r}_1 - \vec{r}_2|} |ij\rangle. \quad (\text{S4})$$

Considering the scaling invariance of the Dirac equation, we rescale our results down to the experimental field strength ($l_B \propto 1/\sqrt{B}$). Effectively, our results thus correspond to an $\approx 330 \times 330$ nm²-sized flake. We evaluate both contributions for all pairs of eigenstates. The state indices i and j can each be split into a Landau level index $\pm n$ and a quantum number m , that labels the degenerate states, as described in the main manuscript, i.e., $i = (\pm n, m)$, $j = (\pm n', m')$. Eigenstates are assigned to specific Landau levels $\pm n$ and $\pm n'$ based on their energy. Due to the finite size of our system, there are a few states within the energy gaps between the Landau levels, which we do not include in the evaluation of the self energy.

TEMPERATURE-DEPENDENT SHUBNIKOV-DE-HAAS OSCILLATIONS

To extract the renormalization of v_F at low magnetic fields, we closely follow the method used by Elias *et al.* [13] and perform temperature-dependent Shubnikov-de Haas oscillation measurements. We measure the conductivity σ as

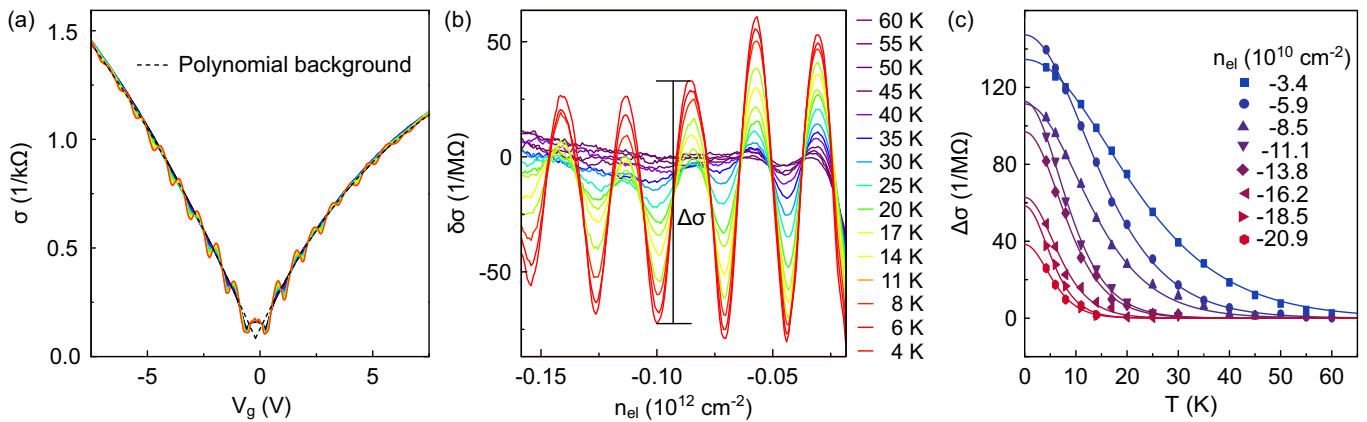


FIG. S3. (a) Electrical conductivity as a function of applied gate voltage V_g for different temperatures at a magnetic field of $B = 0.25$ T. The dashed line represent a fit of a polynomial background for both electron and hole doping. (b) Shubnikov-de Haas oscillations at $B = 0.25$ T after subtraction of a polynomial background. (c) Height of the oscillations $\Delta\sigma$ as a function of temperature for different charge carrier densities.

a function of charge carrier density for different temperatures in a range of $T = 4$ K to $T = 60$ K at a magnetic field of $B = 0.25$ T (see Fig. S3a). For electrons and holes we separately fit a 4th-order polynomial to the smooth, high temperature data and subtract this background from all measurements. The resulting conductivity oscillations $\delta\sigma$ are shown exemplary in Fig. S3b for the hole side. We extract the amplitude of the Shubnikov-de Haas oscillations as the difference $\Delta\sigma$ between maxima and minima (see label in Fig. S3b). This makes the extracted amplitude almost independent of the chosen background. The amplitude as a function of temperature (T) for different hole densities are presented in Fig. S3c. The amplitude follow the Lifshitz-Kosevich formula [42]:

$$\Delta\sigma \propto T / \sinh\left(2\pi^2 k_B T \frac{m_c}{e\hbar B}\right), \quad (\text{S5})$$

where $m_c = \hbar\sqrt{\pi n_{el}}/v_F$ is the cyclotron mass at a given n_{el} . By fitting this expression to our data (see Fig. S3c), we are able to extract v_F for different charge carrier densities, which is shown in the inset in Fig. 3 in the main text.

FINITE RENORMALIZATION OF THE FERMI VELOCITY IN PRESENCE OF LANDAU LEVELS

As shown by González *et al.* [9], for two-dimensional massless Dirac fermions interacting via the Coulomb potential, the Fock contribution to the Fermi velocity is logarithmically divergent in the limit of zero temperature and chemical potential. The corresponding Fock contribution to the Hamiltonian is:

$$\hat{H}_F = \sum_{\vec{k}} \sum_{\alpha, \beta} \hat{\Psi}_{\alpha}^{\dagger}(\vec{k}) h_{\alpha\beta}(\vec{k}) \hat{\Psi}_{\beta}(\vec{k}), \quad (\text{S6})$$

where $\hat{\Psi}_{\beta}(\vec{k})$ is the annihilation operator for the Dirac fermion with the quasi-wave vector \vec{k} and pseudospin projection β ,

$$h_{\alpha\beta}(\vec{k}) = -2\pi e^2 \sum_{\vec{k}'} \frac{\rho_{\beta\alpha}(\vec{k}')}{|\vec{k} - \vec{k}'|}, \quad (\text{S7})$$

and $\rho_{\beta\alpha}(\vec{k}) = \langle \hat{\Psi}_{\vec{k}\alpha}^{\dagger} \hat{\Psi}_{\vec{k}\beta} \rangle$ is the single-particle density matrix ([43], Sect. 8.4). Its spinor structure is given by the expression:

$$\hat{\rho}_{\vec{k}} = n_{\vec{k}} \hat{I} + \vec{m}_{\vec{k}} \hat{\sigma}, \quad (\text{S8})$$

where \hat{I} is the 2×2 unit matrix, $\hat{\sigma}$ are the Pauli matrices and the pseudospin density $\vec{m}_{\vec{k}}$ has the form $\vec{m}_{\vec{k}} = \vec{k}F(k)$. Following Ref. [43], Sect. 7.2, for chemical potential and temperature equal to zero

$$F(k) = \frac{1}{2k}. \quad (\text{S9})$$

Then the Fock contribution to the Fermi velocity reads ([43], Sect. 8.4):

$$\delta v_F = \frac{\pi e^2}{\hbar} \sum_{\vec{k}} \frac{F(k)}{k} = \frac{e^2}{2\hbar} \int_0^\Lambda dk F(k), \quad (\text{S10})$$

where $\Lambda \propto 1/a$ is the ultraviolet (UV) cutoff due to the inapplicability of the Dirac model at large wave vectors and a is the interatomic distance of the graphene lattice. Explicit numerical calculations on a lattice for the case of a pure Coulomb interaction [44] give the value $\Lambda \approx 0.8/a$. When substituting Eq. S9 into Eq. S10 we have a divergence at the lower limit, which, at finite charge carrier density, is cut off at the Fermi wave vector k_F . The result reads:

$$\delta v_F = \frac{e^2}{4\hbar} \ln \left(\frac{\Lambda}{k_F} \right). \quad (\text{S11})$$

In the presence of a magnetic field, the density matrix Eq. S8 and therefore the function $F(k)$ can be calculated using the explicit expression for the Green's function of massless Dirac electrons in the presence of a magnetic field found in Ref. [45]. The result is

$$F(k) = \frac{l_B}{2\sqrt{\pi}} \int_0^\infty ds \frac{\exp(-k^2 l_B^2 \tanh(s))}{\sqrt{s} \cosh(s)^2}, \quad (\text{S12})$$

where $l_B = \sqrt{\hbar/(eB)}$ is the magnetic length. Substituting Eq. S12 into Eq. S10 and changing the order of integrations we obtain

$$\delta v_F = \frac{e^2}{8\hbar} \int_0^\infty ds \frac{\text{erf}(\Lambda l_B \sqrt{\tanh(s)})}{\sqrt{s} \tanh(s) \cosh(s)^2}, \quad (\text{S13})$$

where

$$\text{erf}(x) = \frac{2}{\sqrt{\pi}} \int_0^x ds \exp(-s^2) \quad (\text{S14})$$

is the error function. Assuming that $\Lambda l_B \gg 1$, one can calculate the integral in Eq. S13 by splitting the integration interval into two parts: $(0, \infty) = (0, C) + (C, \infty)$ with some $1/(\Lambda l_B)^2 \ll C \ll 1$. With logarithmic accuracy, one has, instead of Eq. S11,

$$\delta v_F = \frac{e^2}{4\hbar} \ln(\Lambda l_B). \quad (\text{S15})$$

Thus the infrared divergence (Eq. S11) is cut off at wave vectors on the order of the inverse magnetic length and the dependence of the Fermi velocity on the electron filling factor is no longer singular in the presence of a magnetic field.